An Improved Dispatchable Wind Turbine Generator and Dual-Battery Energy Storage System to Reduce Battery Capacity Requirement

Yang Li, S. S. Choi and D. M. Vilathgamuwa
Queensland University of Technology
School of Electrical Engineering and Computer Science
Brisbane, Australia
Email: y245.li@qut.edu.au

D. L. Yao
Nanyang Technological University
School of Electrical and Electronic Engineering
Singapore
Email: yaod0002@e.ntu.edu.sg

***Abstract*— This paper examines an improved dual-battery energy storage scheme designed to achieve wind power dispatchability. The capacity of the battery energy storage system is greatly reduced by allowing direct power flow from wind turbine generator to the grid via a dc bus, as the two batteries interchange their charging and discharging roles at specific time. The method to determine the optimal capacity of the energy storage system is given, and is based on the characteristics of the battery and long-term wind power profile. Numerical examples show the validity of the proposed schemes.**

Keywords—Wind energy conversion system; battery energy storage system; dispatchability; battery capacity determination

I. INTRODUCTION

The desire for clean and renewable energy leads to the rapid development of the wind energy conversion system (WECS) in the past decades. Wind generation is one of the most crucial renewable energy technologies, and it plays an important role in the global electricity supply market [1]. As the penetration level of WECS in power grids increases, however, the negative impact of the intermittent wind power to the grids becomes less and less trivial an issue. Fortunately the use of battery energy storage system (BESS) is one promising solution to the large-scale wind power integration problem [2], in terms of its functionalities in power levelling, power bridging and power quality improvement. Indeed amongst the various BESS schemes designed to operate in conjunction with WECS, the dual-battery system shown in Fig. 1 for the direct-driven wind turbine generator (WTG) is promising as it can lead to the dispatchability of wind power [3].

In this dual-battery scheme, one of the two batteries, say B1 will act as the stand-by battery to absorb the unsteady wind power P_w from the WTG via the machine-side converter (MSC) and the dc/dc converter 1, i.e., $P_{b1} = P_w$. At the same time, the other battery B2, which is called the in-service battery, discharges and delivers pre-determined level of power P_d to the grid via the dc/dc converter 2 and the grid-side converter (GSC). Thus $P_{b2} = -P_d$. If the discharging time T_d of the in-service battery B2 can be controlled to be equal to the charging time T_c of the stand-by battery B1, the mechanically control switches (MCSs) can be activated to interchange the roles of the two batteries and the above-mentioned cycle is repeated. In this scheme, wind speed forecast is important in determining the value of the dispatched power P_d, and scheduling and updating of P_d is necessary to make sure that 1) the changeover is to occur so as to fully utilize the storage capacity of the BESS; 2) specific dispatch requirement is met; 3) objectives are met such as to maximize the economic benefit of the dispatch. Fully charged/discharged cycles can be obtained, which is demonstrated to be an effective way to prolong the battery lifetime [4].

Although this dual-battery scheme for WECS is effective to provide dispatchability and to alleviate the power quality problem caused by the fluctuating wind power, the two battery banks need to be of relatively large capacity. This is because to provide continuous power flows for both the input and output sides, the two groups of MCSs must operate simultaneously. The active power in this system can only flow in two manners: either as the black dotted lines or the grey dashed lines shown in Fig. 1. This control strategy creates complete isolation between the WTG and the grid, which solves the power quality problems caused by the fluctuating P_w. However, as would be shown later, a considerable portion of the wind power has to flow unnecessarily through the two batteries. This requires an increase in the BESS capacity. The unnecessary power flows also reduce the overall efficiency of the energy conversion process and the lifetime of the batteries.

Another related issue is that in practice, one can expect the output power from an aggregation of WTG to be much smoother than that from a single WTG. This is due to the spatial smoothing effect and it is a desirable outcome. Also, the impact of the

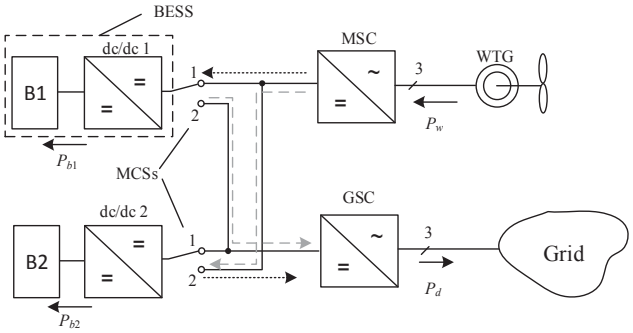

Fig. 1. Dual-battery configuration using MCSs in a grid-connected wind farm proposed in [3]. The solid arrows show the reference directions of power flows.

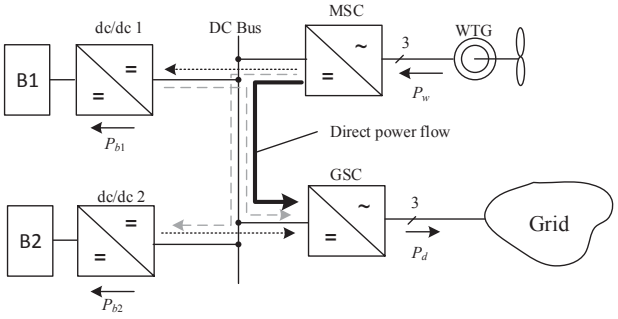

Fig. 2. Improved dual-battery configuration using a dc bus in a grid-connected wind farm. The solid arrows show the reference directions of power flows.

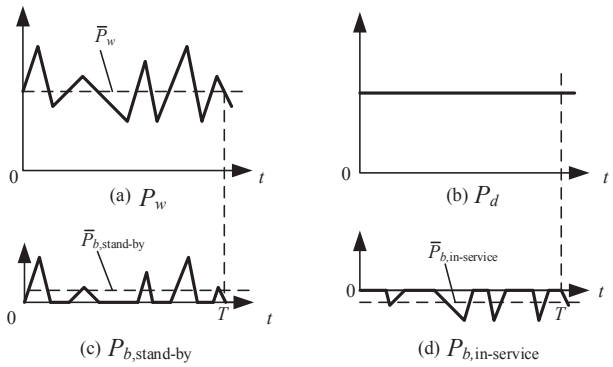

Fig. 3. Decomposition of input wind power P_w in (a) to constant grid power of (b), the stand-by battery power $P_{b,\text{stand-by}}$ of (c) and the in-service battery power stand-by battery power $P_{b,\text{in-service}}$ of (d).

aggregated WTG output power to the grid can be reduced further with the help of well-established power electronics technologies. Thus, with these factors in mind, it is plausible to consider the establishment some direct power flows path from the WTG to the grid. This is with the view to reduce the BESS capacity, while still retain the dispatchability benefits derived from the scheme shown in Fig. 1.

II. Preliminary Considerations

Recognizing the limitation imposed by the MCSs, an improved scheme of the dual-battery energy storage system for a wind farm is proposed and shown in Fig. 2. In comparison to the original scheme shown in Fig. 1, the MCSs are replaced by a dc bus which collects the dc power from a number of MSCs and provide a direct power flow path from the WTGs to the grid (as indicated by the black solid line in Fig. 2). It is equivalent to the connection of two BESSs to the dc-link of a conventional ac/dc/ac back-to-back converter for a direct-driven WTG. The schematics in Fig. 2 can also represent a wind farm where the GSC may be located some distance from an aggregation of WTG and MSC such as in the case of an offshore wind farm. As such, the dc bus represents the high-voltage dc collector and undersea cables, while large-scale BESS and GSC can be designed for smoother dc power injection and are installed on-shore to reduce the installation and maintenance costs.

In the context of dispatchability, the objective of the proposed scheme is to deliver committed constant power P_d to the grid within the dispatch interval (bid interval) x hour a day or so ahead while subjecting to the stochastic input power P_w. Often x is one [5] or two [3, 6] . The two batteries will cooperate to compensate for the power difference $P_d - P_w$. Similar to the scheme in [3], it is assumed the two batteries B1 and B2 have identical characteristics and capacity.

Without loss of generality, assume at the beginning of the investigated charging/discharging cycle, B1 is empty i.e., its state-of-charge (SOC) is $SOC_1 = SOC_{min}$ and it is ready to be charged. At the same time, B2 is fully charged ($SOC_2 = SOC_{max}$) and is ready to discharge. If $P_w > P_d$, P_d will be completely provided by the power flow from the MSC, and the surplus power $P_w - P_d$ will charge B1. B1 is called the *stand-by battery*. In this period, B2 will rest and the dc/dc converter 2 will be blocked. On the other hand, if $P_w < P_d$, B2, which is called the *in-service battery*, will discharge and compensate for the difference $P_d - P_w$. In this period, the dc-dc converter 1 will be blocked and B1 will rest. In this stage, the directions of power flow of the two batteries are indicated by the black dotted arrows in Fig. 2 when the batteries are not in the "rest" state. If the charging time T_{c1} of B1 is exactly the same as the discharging time T_{d2} of B2, B1 and B2 will interchange their roles and in the next half-cycle B1 becomes the in-service battery and B2 becomes the stand-by battery. In this stage, the directions of power flows of the batteries are indicated by the grey dashed arrows in Fig. 2.

In general, at the k^{th} time interval, the control strategy can be described by the following equations, i.e.

$$P_{b,\text{stand-by}}(k) = \begin{cases} P_w(k) - P_d, & P_w(k) > P_d \\ 0, & P_w(k) \le P_d \end{cases} \quad (1)$$

$$P_{b,\text{in-service}}(k) = \begin{cases} 0, & P_w(k) \ge P_d \\ P_d - P_w(k), & P_w(k) < P_d \end{cases} \quad (2)$$

For ease of analysis of the strategy, the power losses of the converters and batteries are not considered. According to (1) and (2), P_w can be decomposed into three components as illustrated in Fig. 3: the committed constant power P_d, the charging or stand-by battery power $P_{b,\text{stand-by}}$ and the discharging or in-service battery power $P_{b,\text{in-service}}$. It can be seen that, over the period $T = mx$ hours ($m = 1,2,3\ldots$), if the committed power P_d in T, denoted as $P_{d,T}$, equals to the average wind power $\bar{P}_{w,T}$ in the same period, the stand-by battery would absorb the same amount of energy as that discharged by the in-service battery. So denote the average values of $P_{b,\text{stand-by}}$ and $P_{b,\text{in-service}}$ by $\bar{P}_{b,T}$, and $E_{b,T}$ is the total charged/discharged energy in the period T,

$$\bar{P}_{b,\text{stand-by}} = -\bar{P}_{b,\text{in-service}} = \bar{P}_{b,T} \quad (3)$$

$$E_{b,\text{stand-by}} = -E_{b,\text{in-service}} = E_{b,T} \quad (4)$$

The values of $P_{d,T}$, $\bar{P}_{w,T}$, $\bar{P}_{b,T}$ and $E_{b,T}$ are dependent of the selection of T. Thus, the value of T is important in the determination of the capacity of the BESS. $P_{d,T}$ must be determined and submitted to the grid or transmission system

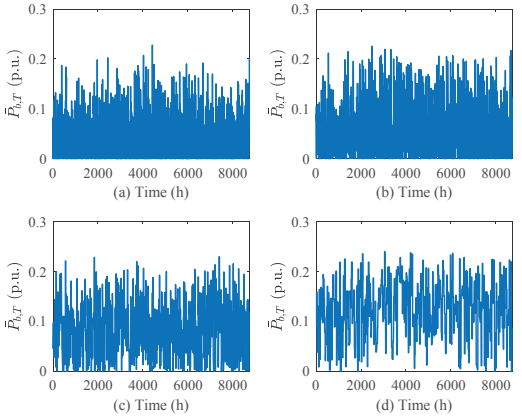

Fig. 4. Time-series of $\bar{P}_{b,T}$ obtained for aT of (a) 1 h (b) 4 h (c) 12 h (d) 24 h.

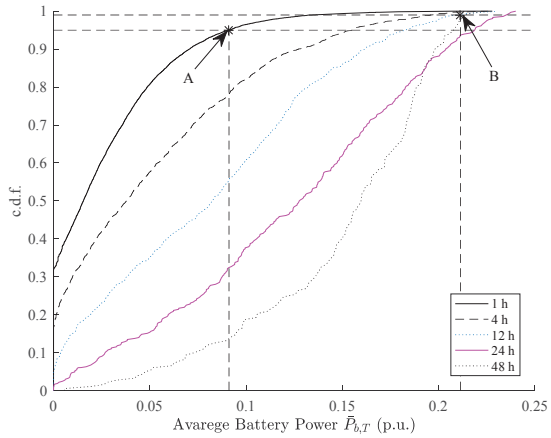

Fig. 5. Cumulative distribution function of $\bar{P}_{b,T}$ at various T.

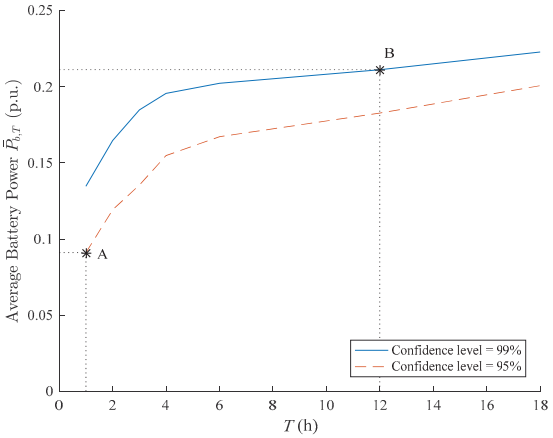

Fig. 6. Selection of $\bar{P}_{b,T}$ based on confidence level and T.

operator 12 or 24 hours in advance. For such short-term dispatch planning, the reliability of the dispatch plan depends very much on the wind speed forecasting technique used and the selected averaging period T. If T is infinitely large, $P_{d,T}$ will approach the long-term statistical expected value $\bar{P}_{w,\infty}$ of the wind power.

Although forecast error is inevitable, this paper shall begin from the most ideal case when perfect prediction of wind power is assumed. The impact of the forecast error on the performance of the system shall be studied in the later part of the paper.

III. Analysis And Design

A. Distribution Function of $\bar{P}_{b,T}$

As alluded to earlier, the average battery power $\bar{P}_{b,T}$ can be obtained by averaging $P_{b,\text{stand-by}}$ within the period T, as shown in Fig. 3 (c). $\bar{P}_{b,T}$ for a given T can be calculated according to

$$\bar{P}_{b,T} = \frac{1}{2N}\sum_{k=1}^{N}\sqrt{\left(P_w(k) - \frac{1}{N}\sum_{k=1}^{N}P_w(k)\right)^2} \tag{5}$$

where N is the number of samples in T. If $T = +\infty$, it can be seen that

$$\bar{P}_{b,T} = \bar{P}_{b,\infty} = \sigma_\infty / 2 \tag{6}$$

where σ_∞ is the standard deviation of the wind power.

Using (5), Fig. 4 shows $\bar{P}_{b,T}$ of a fictitious wind farm derived from a 1-year wind speed v_w data-set extracted from [7] and for various values of T. The normalized wind turbine power P_w is calculated by assuming the simplified power curve of the wind turbine:

$$P_w(k) = \begin{cases} 0, & v_w(k) \le v_{\text{cut-in}} \text{ or } v_w(k) > v_{\text{cut-out}} \\ \left(\dfrac{v_w(k)}{v_{\text{rated}}}\right)^3, & v_{\text{cut-in}} < v_w(k) \le v_{\text{rated}} \\ 1, & v_{\text{rated}} < v_w(k) \le v_{\text{cut-out}} \end{cases} \tag{7}$$

where $v_{\text{cut-in}}$ and $v_{\text{cut-out}}$ are the cut-in and cut-out wind speeds respectively, and v_{rated} is the wind speed at the rated power P_w = 1.0 p.u. Additionally, a moving average smoothing effect is assumed to reflect the diversity between the output power of the WTG units in the wind farm. Theoretically, the battery should be designed to meet the peak power requirement shown in Fig. 4. However, high value $\bar{P}_{b,T}$ rarely occurs as can be seen from Fig. 5. The figure shows the cumulative distribution functions (cdf) of $\bar{P}_{b,T}$ for different T. From the cdf, one can readily determine the value of $\bar{P}_{b,T}$ at the corresponding probability level, although Fig. 4 and Fig. 5 show that the maximum values of $\bar{P}_{b,T}$ are similar at 0.22~0.23 p.u. at different T.

From Fig. 5, it can also be seen the cdf at $\bar{P}_{b,T} = 0$ is not zero for small T. The probability$\bar{P}_{b,T}$ is zero decreases as T increases. For the consideration of short-term dispatch, however, the case of $T \le$12 h has been adopted for further analysis. Fig. 6 shows $\bar{P}_{b,T}$ as a function of T under two selected probability or confidence levels. Clearly by reducing the confidence level or the value of T, the threshold value selected for $\bar{P}_{b,T}$ used in determining the BESS capacity can be lowered. For example, $\bar{P}_{b,T}$ can be reduced by a factor of more than 2 if the confidence level is reduced from 99% to 95% and T is reduced from 12 h to 1 h, corresponding to moving from B to A of Fig 6.

B. Minimum BESS Capacity

Similar to the approach described in [3], let the maximum allowable charge/discharge power per battery cell be $P_{c,o}$. Thus, the minimum number of cells in the BESS required to charge/discharge $\bar{P}_{b,T}$ is

$$n_0 = \bar{P}_{b,T} / P_{c,o} \tag{8}$$

Thus, the minimum required BESS capacity can be simply expressed as $n_0 C_{p,r}$ where $C_{p,r}$ is the rated ampere-hour capacity of a cell.

Next, compare the minimum required BESS capacity determined in (8) with that shown in [3]. Denoting the long-term average wind power as $\bar{P}_{w,\infty}$, the minimum number of cells n'_0 required in the scheme proposed in [3] is

$$n'_0 = \bar{P}_{w,\infty} / P_{c,o} \tag{9}$$

A factor κ is defined next as the ratio of n'_0 to n_0, i.e.

$$\kappa = n'_0 / n_0 = \bar{P}_{w,\infty} / \bar{P}_{b,T} \tag{10}$$

A κ with value greater than unity shows the minimum required battery capacity is reduced if the present approach is adopted. Based on the same wind power data used to derive Fig. 4-6, Fig. 7 shows the value of κ as a function of $\bar{P}_{w,\infty}$ and $\bar{P}_{b,T}$. The boundary for κ=1 in the figure divides the surface into two regions. From Fig. 5, the cdf shows that $\bar{P}_{b,T}$ does not exceed 0.25 p.u. for κ=1. So if $\bar{P}_{w,\infty}$ is greater than 0.25 p.u., the proposed scheme will always reduce the minimum required BESS capacity by the factor κ. The long-term average power $\bar{P}_{w,\infty}$ is equal to the capacity factor of the wind farm, which is normally expected to be high when determining the wind farm site. For example, the average capacity factor globally is around 0.35 p.u. and can range from 0.2 to 0.4 p.u. [8], and has the potential to increase to 0.6 p.u. in the future [9].

C. Number of Averaging Period T Per Charging/Discharging Half-Cycle

The maximum usable stored energy in a battery cell can be estimated as

$$\Delta E_{\text{cell}} = E_{\max} - E_{\min} = C_{p,r}(\text{SOC}_{\max} V_{\max} - \text{SOC}_{\min} V_{\min}) \tag{11}$$

where $E_{\max}$ and $E_{\min}$ are the maximum and minimum stored energy, $C_{p,r}$ is the rated ampere-hour capacity of one cell, $V_{\max}$ and $V_{\min}$ are the maximum and minimum cell voltage.

Thus, once the minimum required number of cells n_0 is determined using the method given in Section III.A, the total usable energy in the BESS is also known. With the average battery power $\bar{P}_{b,T}$, then using (8) and (11), the minimum half-cycle charging/discharging time $T_{\text{hc,min}}$ can be estimated as

$$T_{hc,\min} = \frac{n_0 \Delta E_{\text{cell}}}{\bar{P}_{b,T}} = \frac{C_{p,r}(\text{SOC}_{\max} V_{\max} - \text{SOC}_{\min} V_{\min})}{P_{c,o}} \tag{12}$$

Equation (12) shows that $T_{hc,\min}$ is determined by the capacity and voltage ratings of the cell and is independent of the selection of T. If the actual average battery power within a particular interval T is less than the selected $\bar{P}_{b,T}$ used in the BESS capacity calculation, the charging/discharging time within this interval will be longer than $T_{hc,\min}$. The minimum number of averaging period T per charging/discharging half-cycle can be obtained from

$$N_{\min,T} = \frac{T_{hc,\min}}{T} = \frac{C_{p,r}(\text{SOC}_{\max} V_{\max} - \text{SOC}_{\min} V_{\min})}{P_{c,o} T} \tag{13}$$

As after one averaging period T, the two batteries will charge/discharge the same amount of energy, it is desirable to have an integer number of T periods within a charging/discharging half-cycle. This is so that the total amount of discharged and charged energy in the two BESSs can be the same. Thus, it means smaller T or larger $N_{\min}$ can provide an increased opportunity to realize the above-mentioned condition.

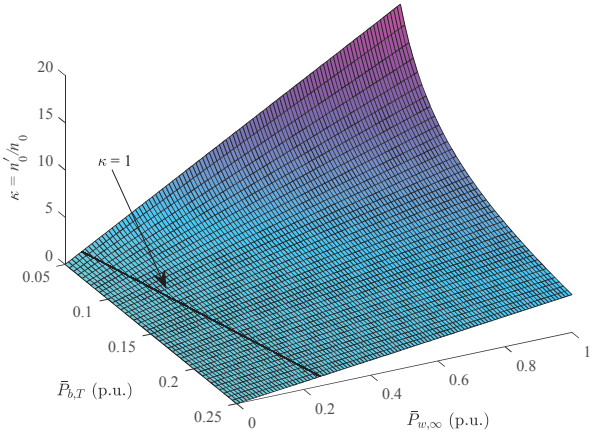

Fig. 7. Reduction of BESS capacity for different $\bar{P}_{w,\infty}$ and $\bar{P}_{b,T}$.

D. Mitigation of Non-Optimal Changeover

In practice however, it is inevitable there would be a non-integer number of T periods within a charging/discharging half-cycle. As long as one BESS reaches its SOC limit and requires it to change its role, the remaining BESS must also change its role at the same time regardless of whether it has reached its SOC limit. This "non-optimal" changeover is unacceptable as the battery capacity used will continue to shrink and the battery voltage limit would be exceeded.

In order to overcome this problem, the control strategy shown on Fig. 8 is proposed to regulate the dispatch power P_d in advance. Once the system observes that the SOC of either battery reaches its pre-defined upper threshold or lower threshold levels (SOC_U and SOC_L), the system would adjust P_d in the next dispatch intervals to balance the pace of the charging/discharging process. In Fig. 8, i is the index number of the dispatch interval. When this algorithm is activated, P_d is updated in every dispatch interval. The adjusted dispatched power ΔP_d is proportional to the difference of $|\text{SOC}_{\max} - \text{SOC}_{\text{stand-by}}|$ and $|\text{SOC}_{\text{in-service}} - \text{SOC}_{\min}|$, where $\text{SOC}_{\text{stand-by}}$ and $\text{SOC}_{\text{in-service}}$ are the SOC of the stand-by and in-service batteries respectively. The proportional gain K_p determines the speed of this "synchronization" process.

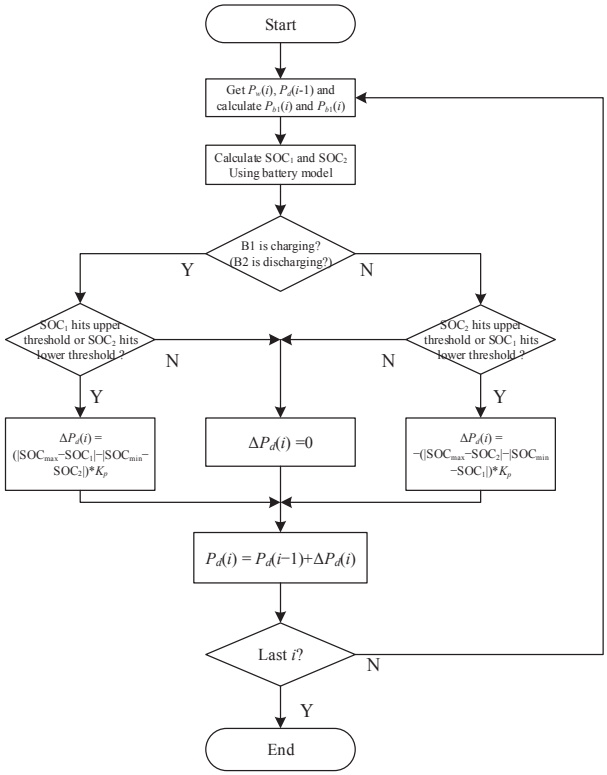

Fig. 8. P_d updating algorithm to synchronize the two batteries.

IV. Numerical Examples

A. Case Study

A set of 48-hour wind power data was derived from the recorded wind speed data-set reported in [7] and alluded to in the previous section. The wind power profile is as shown in Fig. 8. The forecasted wind speed error is assumed to be normally distributed [6] and has the mean μ_f = 0.1 p.u. and standard deviation σ_f = 0.1 p.u. of its rated wind speed. The power rating of the fictitious wind farm is assumed to be 100 MW. NaS battery cell is used in the case study, although other types of batteries may also be considered. The model of NaS cell is given in [3] with the following parameters: $P_{c,o}$ = 88.09 W, $C_{p,r}$ = 610 Ah, V_{max} = 2.25 V, V_{min} = 1.75 V, SOC_{max} = 100%, SOC_{min} = 20%.

With the long-term wind turbine power data, the expected average wind power $\bar{P}_{w,\infty}$ was found to be 0.5106 p.u. For the proposed scheme, if the 95% confidence level were to be selected and T = 1 h, according to Fig. 6, $\bar{P}_{b,T}$=0.09 p.u. at point A. Thus, according to (10), κ = 0.5106/0.09 = 5.67. On the other hand, if the confidence level is 99% and T = 12 h, $\bar{P}_{b,T}$=0.215 p.u. at point B and the corresponding κ = 0. 5106/0.215 = 2.37.

For the first case, the number of cells for the scheme shown in [3] and that of the proposed scheme can be obtained using (8) and (9) respectively, i.e.

$$n_0' = (0.5106\times100\times10^6)/88.09 = 574353 \quad (14)$$

$$n_0 = (0.09\times100\times10^6)/88.09 = 101237 \quad (15)$$

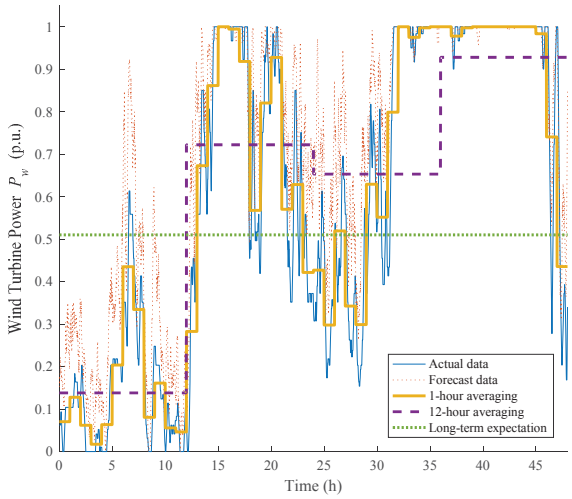

Fig. 9. Normalized wind turbine power P_w in 48 h.

The minimum capacity of the BESS of the proposed scheme is 6.175×10^7 Ah or 139 MWh. In this case, n_0E_{max} = 139 MWh (57.9 p.u. of rated power for 1 minute) and n_0E_{min} = 21.6 MWh (9.0 p.u.×min). The minimum charging/discharging half-cycle time can be calculated using (12) as

$$T_{hc,min} = \frac{610\times(1\times2.25-0.2\times1.75)}{88.09} = 13.157 \text{ h} \quad (16)$$

Thus, according to (13), in one half-cycle, there are at least 13.157 T-periods or dispatch intervals for T = 1 h. Thus, $N_{min,1}$ = 13.157. Similarly, for the case of T = 12 h, it can be readily calculated that n_0 = 244069, n_0E_{max} = 335 MWh (139.6 p.u.×min) and n_0E_{min} = 52.1 MWh (21.7 p.u.×min) and $N_{min,12}$ = 1.1.

The averaging of P_w for various T is also shown in Fig. 9. As the analysis is based on the assumption of perfect wind speed prediction, the averaging power is treated as the constant committed power P_d that will be submitted to the grid operator. Therefore, the control strategy given in (1) and (2) can be applied with the known P_w and P_d.

The simulation results for T = 1 h and T = 12 h are shown in Fig. 10 and Fig. 11 respectively, where the SOC of the two batteries and the average power/dispatched power are shown. The results without and with forecast error are shown in the subplots (a) and (b) respectively. It can be seen at any time only one BESS is charging/discharging, while the other BESS remains at rest and its SOC is thus constant. The actual number of T in the first half-cycle are 20 and 2 for the two cases respectively. Comparing to the $N_{min,1}$ = 13.157 and $N_{min,12}$ = 1.1 calculated previously using (13), the larger N here is due to the fact that the average power deviation in the investigated period is smaller than the maximum averaging power deviation determined by Fig. 6.

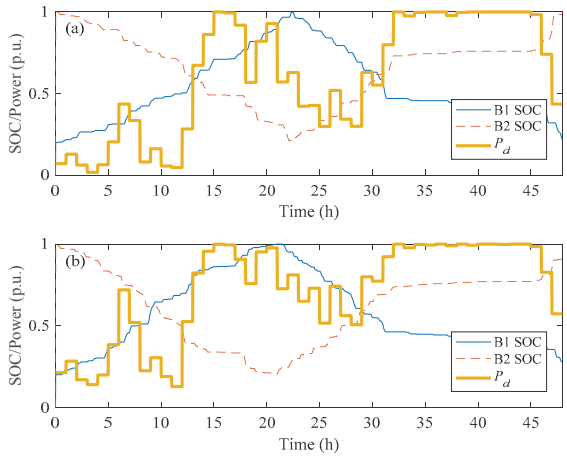

Fig. 10. Battery SOC in accordance to the wind power profile shown in Fig. 9 (T = 1 h): (a) no forecast error (b) with forecast error.

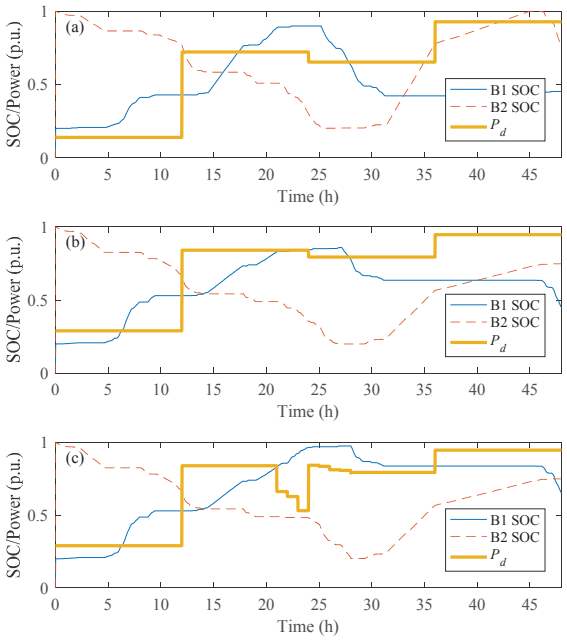

Fig. 11. Battery SOC in accordance to the wind power profile shown in Fig. 9 (T = 12 h): (a) no forecast error and non-optimal BESS changeover; (b) with forecast error, but non-optimal BESS changeover; (c) with forecast error and optimal BESS changeover.

B. Mitigation of Non-Optimal Changeover

It can clearly be observed that the two BESSs do not always reach the full and empty states at the same time. For instance, in Fig. 11 (b) at time t = 26 h, at this changeover, when B2 is fully discharged, B1 has just reached about 75% SOC. As explained earlier, this is a result of non-integer number of T in a half-cycle. The outcome of the simulation study, when the re-synchronization of the BESS algorithm of Fig. 8 has been applied, are shown in Fig. 11 (c). It can be observed that at t = 21 h, the algorithm is activated as the system has detected that the SOC of B1 has reached the upper threshold SOC_U = 80%, while the SOC of B2 is only 50%. In the optimal changeover strategy, SOC of B2 is to reach the lower SOC threshold of about SOC_L = 40% at the same time. Thus, P_d is reduced in the next dispatch interval. In doing so, the charging process is sped up and the discharging process is slowed down. This online updating of P_d will only be terminated when the paces of the SOC variation of the charging battery and the discharging battery are the same.

V. Conclusions

In this paper an improved scheme of a dual-battery dispatchable WTG-BESS is proposed in order to reduce BESS capacity. From the theoretical analysis and numerical examples, it can be seen that the introduction of the dc bus provides the potential to effectively reduce the minimum capacity requirement of the BESS through considering the statistical characteristics of the wind speed. The method to determine the BESS capacity and the mechanism to obtain the optimal changeover of the two batteries are proposed to ensure safe operation of BESS. The reduced number of battery cells, lower dc/dc converter rating and removal of the MCSs can decrease the cost of the dual-battery WTG-BESS, while the dispatchability of the system can still be achieved. It thus retains the potential to further maximize the wind farm economic benefit, through well-designed dispatch strategy.

Acknowledgment

This work was supported by the Australian Research Council Discovery Grant DP160101325.

References

[1] B. Wu, Y. Lang, N. Zargari, and S. Kouro, *Power Conversion and Control of Wind Energy Systems*. Hoboken, NJ: Wiley, 2011.

[2] G. Boyle, *Renewable Electricity and the Grid: The Challenge of Variability*. London: Earthscan, 2007.

[3] D. L. Yao, S. S. Choi, K. J. Tseng, and T. T. Lie, "A statistical approach to the design of a dispatchable wind power-battery energy storage system," *IEEE Trans. Energy Convers.*, vol. 24, no. 4, pp. 916-925, Dec. 2009.

[4] Q. Jiang, Y. Gong, and H. Wang, "A battery energy storage system dual-layer control strategy for mitigating wind farm fluctuations," *IEEE Trans. Power Syst.*, vol. 28, no. 3, pp. 3263-3273, Aug. 2013.

[5] S. Teleke, M. E. Baran, S. Bhattacharya, and A. Q. Huang, "Optimal control of battery energy storage for wind farm dispatching," *IEEE Trans. Energy Convers.*, vol. 25, no. 3, pp. 787-794, Sep. 2010.

[6] Q. Li, S. S. Choi, Y. Yuan, and D. L. Yao, "On the determination of battery energy storage capacity and short-term power dispatch of a wind farm," *IEEE Trans. Sustain. Energy*, vol. 2, no. 2, pp. 148-158, Apr. 2011.

[7] *1-minute Interval Iowa AWOS data* (n.d.) [Online]. Available: http://mesonet.agron.iastate.edu/request/awos/1min.php

[8] L. Carson, "Australian Energy Resource Assessment," Department of Resources, 2nd ed. Canberra, 2014.

[9] J. Richardson. (2015, May 26). *New Wind Turbine Capacity Factor Could Increase From 40% To 60%.* [Online]. Available: http://cleantechnica.com/2015/05/26/new-wind-turbines-capacity-factor-increase-40-60/